



Contents lists available at ScienceDirect

Journal of Cardiology

journal homepage: www.elsevier.com/locate/jjcc



Original article

Deformability of the pulsating left ventricular wall: A new aspect elucidated by high resolution ultrasonic methods

Motono Tanaka (MD, PhD, FJCC)^{a,*}, Tsuguya Sakamoto (MD, PhD, FJCC)^b,
Shigeo Sugawara (MD, PhD, FJCC)^a, Yoshiaki Katahira (MD, PhD, FJCC)^a,
Kaoru Hasegawa (MD)^a, Hiroyuki Nakajima (RMS)^a, Takafumi Kurokawa (RMS)^a,
Hiroshi Kanai (PhD)^c, Hideyuki Hasegawa (PhD)^c

^a Cardiovascular Center, Tohoku Pharmaceutical University Hospital, Sendai, Japan

^b Hanzomon Hospital, Tokyo, Japan

^c Department of Electrical Engineering, Tohoku University, Sendai, Japan

ARTICLE INFO

Article history:

Received 2 November 2015
Received in revised form 6 January 2016
Accepted 1 February 2016
Available online xxx

Keywords:

Deformability
Contraction-relaxation/extension property
Bellows action
Peristalsis
Pouch-like deformation

ABSTRACT

Background: Although the deformability of the left ventricular (LV) wall appears to be important in maintaining effective cardiac performance, this has not been debated by anyone, probably owing to the difficulties of the investigation.

Objectives: This study applies a new technology to demonstrate how the LV wall deforms so as to adjust for optimum cardiac performance.

Subjects and methods: Ten healthy volunteers were the subjects. Using echo-dynamography, an analysis at the “microscopic” (muscle fiber) level was done by measuring the myocardial axial strain rate (aSR), while the “macroscopic” (muscle layer) level contraction-relaxation/extension (C-R/E) properties of the LV wall were analyzed using high frame rate 2D echocardiography.

Results: Deformability of the LV was classified into three types depending on the non-uniformity of both the C-R/E properties and the aSR distribution.

“Basic” deformation (macroscopic): The apical posterior wall (PW) thickness change was concentric and monophasic, whereas it was eccentric and biphasic in the basal part. This deformation was large in the PW, but small in the interventricular septum (IVS). The elongation of the mitral ring diameter and the downward movement of its posterior part were shown to be concomitant with the anterior extrusion of the PW.

“Combined” deformation (macroscopic and microscopic): This was observed when the basic deformation was coupled with the spatial aSR distribution. Three patterns were observed: (a) peristaltic; (b) bellows-like; and (c) pouch-like.

“Integrated” deformation: This was the time serial aSR distribution coupled with the combined deformation, illustrating the rotary pump-like function.

The deformability of the LV assigned to the apical part the control of pressure and to the basal part, flow volume. The IVS and the PW exhibited independent behavior.

Conclusions: The non-uniformity of both the aSR distribution and the macroscopic C-R/E property were the basic determinants of LV deformation. The apical and basal deformability was shared in LV mechanical function.

© 2016 Japanese College of Cardiology. Published by Elsevier Ltd. All rights reserved.

* Corresponding author at: Cardiovascular Center, Tohoku Pharmaceutical University Hospital, Fukumuro 1-12-1, Miyagino-ku, Sendai 983-8512, Japan.
Tel.: +81 22 719 5161; fax: +81 22 719 5166.

E-mail address: m.tanaka@jata-miyagi.org (M. Tanaka).

<http://dx.doi.org/10.1016/j.jjcc.2016.02.009>

0914-5087/© 2016 Japanese College of Cardiology. Published by Elsevier Ltd. All rights reserved.

Introduction

The deformability of the left ventricular (LV) wall may be an indispensable determinant of smooth and effective LV mechanical performance [1,2]. However, this concept was not noticed by previous researchers. Although it might have been speculated, it would have been difficult to investigate because of the poor spatial

resolution of past investigative methods [3–11], such as X-ray, magnetic resonance imaging (MRI), and conventional 2D echocardiography, including the speckle tracking method. Also, the experimental studies [12–16] and artificial cardiac models [17,18] are not physiological, and cannot observe the phenomena of the living heart moving under “negative pressure” in the thorax [19–24]. The present study attempts to challenge this difficult problem by using the high-resolution non-invasive methodology (echo-dynamography) to confirm the significance of the deformability for LV performance.

Objectives

We attempted to disclose LV wall deformability *in situ* using echo-dynamography which has been heretofore repeatedly described. The “microscopic” method (to the muscle fiber level) measured the axial strain rate (aSR) using the phase difference tracking method [25–29]. The “macroscopic” method (to the muscle layer level) observed the morphology using high frame rate 2D echocardiography. In addition, the spatial and time serial behaviors [7,8,30,31] were observed.

Subjects and methods

Ten presumably healthy volunteers aged 30–50 years (39.6 ± 10.4 years) who had given informed consent were the subjects. They are working in our laboratory, and volunteers with past and present history of adult disease were not included in this study.

Acquisition of the information

The information of the wall dynamics was obtained using the specially designed ultrasonic machine (Aloka 6500 model, Hitachi Aloka Medical, Tokyo, Japan). While the examinee was in the supine or left lateral decubitus position, a transthoracic parasternal 90° sector scan was passed through three points (center of both the aortic and the mitral orifices and the LV apex) so as to include the center of the LV, the left atrium (LA), and both axis lines of the inflow and outflow. This plane was named “longitudinal section plane [32]” and the LV structure was symmetrical with this plane (Fig. 1). The rectangular plane perpendicular to this was named “short-axis plane” throughout which 3D measurement of the LV was done from the apex to base precisely. Then, we measured the intra-ventricular blood flow [30,31] and the LV mechanical phenomena with minimum acoustical measurement error [8,33,34].

Measurement of the macroscopic (muscle layer level) dynamics of the LV wall

A high speed of 66 frame/s with 3.5 MHz in frequency and 4.5 KHz in repetition rate was used for 2D echocardiography [7,8,32]. A 90° scan from the base to the apex was performed.

During one cardiac cycle, the images of continuous 30 frames of every 30 ms were analyzed at each of the 3 points, that is, the apical (A: just above the papillary muscle level), basal (B: ca 10 mm apart from the mitral valve ring), and central (C: in the middle of A and B) (Fig. 1).

The thicknesses of the posterior wall (PW) and the interventricular septum (IVS), and the internal diameter of the LV were measured, respectively. Mitral valve ring diameter (MRD) and the mitral ring movement (MRM) were also measured.

Selected heart rate was about 70/min and the time course of the cardiac cycle of each case was corrected by R–R interval after Bazett's equation to stabilize the data among the subjects.

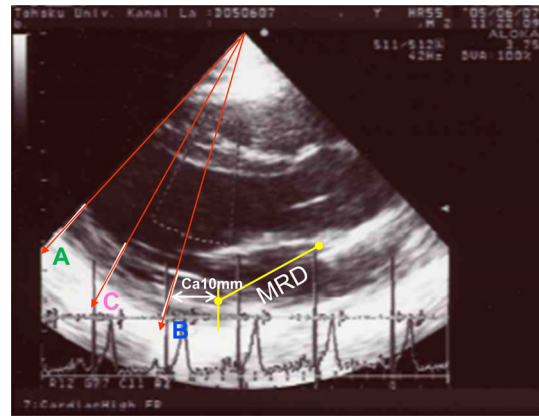


Fig. 1. Measurement methods of the structure change of the LV wall by high frame rate 2D echocardiography and of the high-resolution axial strain rate (aSR) by phase difference tracking method. Cardiac structures confirmed by 2D echocardiogram. The 1–3 beam directions to parts A (apical), C (central), and B (basal) were decided on the long-axis section plane. In the aSR method, the beam direction was decided on the systolic maximum image. The received echo signals from the wall for about 6 s were stocked in the digital memory and processed off-line by using our own developed software. The aSR at the point area on the beam was calculated by the bottom equation (strain rate). Details were shown in the previous papers [35,37]. MRD, mitral ring diameter; US beam, ultrasonic beam; LV, left ventricle; End, endo-cardium; Epi, epicardium; $v(x_{1i}; t)$, velocity at the point of x_{1i} ; $v(x_{2i}; t)$, velocity at the point x_{2i} .

Measurement of the microscopic (muscle fiber level) dynamics of the LV wall by the aSR

For methodological reasons, we measured the myocardial fiber “thickness” change instead of the change in the fiber “length”. This is because the change in the pulsating myocardial fiber length is in inverse proportion to the thickness [21–23], which is easily and accurately measured by the present methodology.

The ultrasound used was 3.75 MHz in frequency and 133 μ s in the pulse repetition interval. The limited angle of each 30° out of 90° was scanned at a high speed of 630 frame/s from the base to the apex (sparse scan) (Fig. 1A–C). The B point was decided from the maximum systolic image. The thickness (821 μ m) was measured at the microscopic level with a high spatial resolution of 200 μ m by using the phase difference tracking method of ultrasound [26,27]. Furthermore, the non-uniformity of the contraction and extension in the local myocardium was estimated from the result of the spatial aSR distribution [25–29,32,35].

The calculated aSR was displayed on the M-mode images. The cold color indicates the increment of the aSR [contraction: aSR(+)] and the warm color, the decrement [extension: aSR(-)]. In this regard, the relaxation (B1) (no active movement) is indicated by black color, where there is nearly no contraction nor extension (the muscle is completely relaxed either in systole or in diastole).

Statistical analysis

The present study did not include a precise statistical analysis. The reasons were as follows:

The inscribed graphs and the measurement values were nearly identical throughout all subjects. There were no visible unavoidable variations in most of the medical study. Mild heart rate variability was present, but it was corrected by Bazett's equation. It was true that individual subjects had slightly different measurement values in the wall thickness and internal dimension, etc., however, the variations are dependent on and parallel to the individual size and dimension. So, to take a mean and deviation of all subjects is meaningless or may be misleading in this study in which all the items had the same changing direction. Essentially, this study was rather "physical" but not physiological or medical, so that it may be

quite difficult to obtain the conclusion if there was variability of the data as seen in the clinical study. The data once stored in the MO-disc gave exactly the same results, whenever it was rechecked by any collaborators, so there was no observer variation- or test-to-test variability. This is the reason why the present article shows only one example in the figures. The authors believe that the limited 10 cases are sufficient to discuss and conclude the results.

Results

When the heart rate was corrected by R-R interval, the time serial changes in the wall thickness and displacement, and the internal diameter during one cardiac cycle showed the same tendency in all cases. Therefore, one example is shown in Fig. 2, and the ratio to the apical data is listed in Tables 1 and 2.

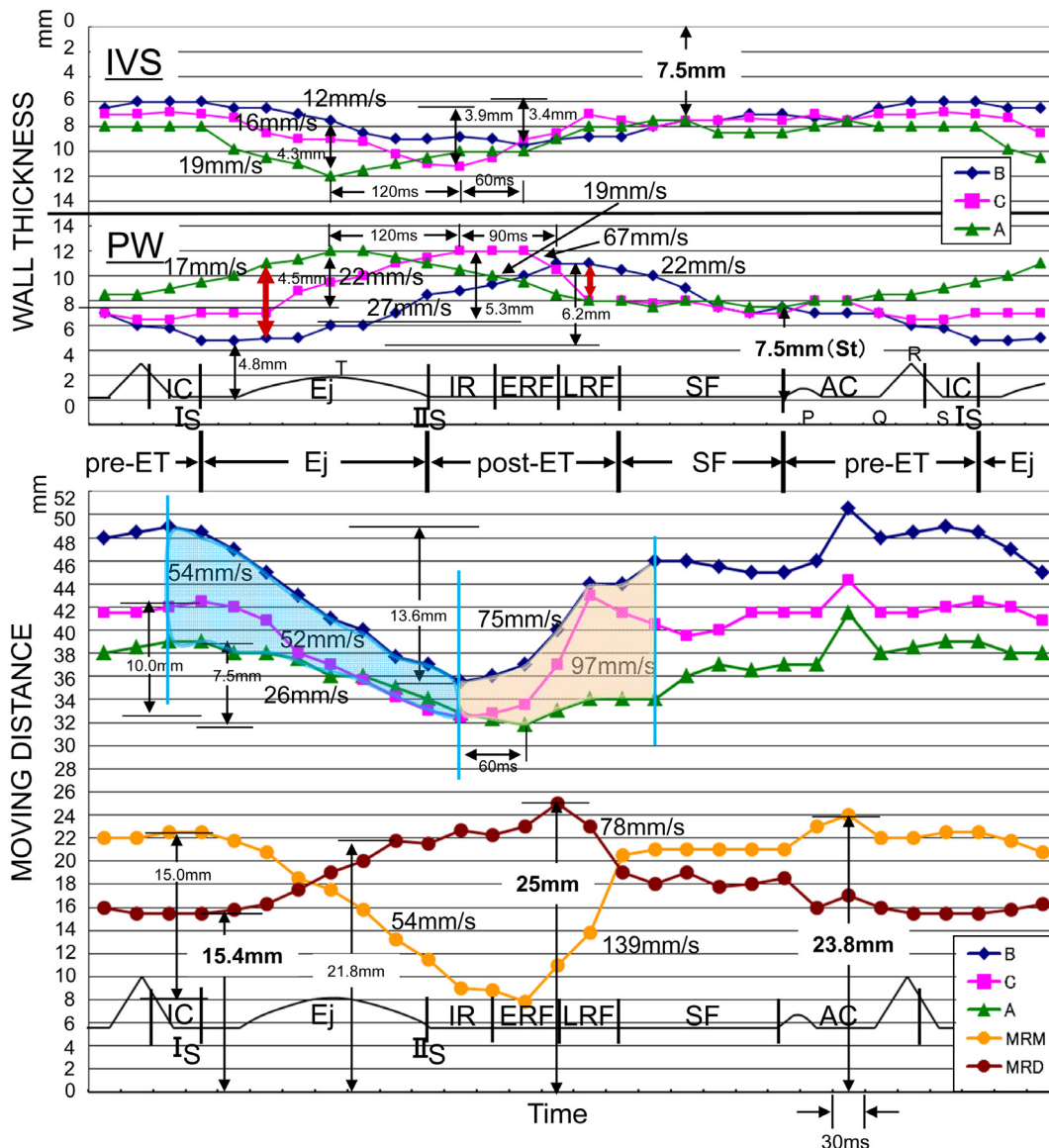


Fig. 2. The various time serial LV changes measured from the successive 30 frames at every 30 ms using long-axis section plane of the high frame rate 2D echocardiograms. Out of the similar measurement values in 10 cases, a representative case is presented. **Top:** Changes in the IVS and PW thickness measured at three parts (A, apical: green triangle; C, central: red square; B, basal: blue rhombus) during cardiac cycle. The numbers indicate the contracting speed of the myocardium (mm/s), the changes of the wall thickness (mm) and the time interval (ms) between the peak point of the contraction in the three parts. The red thick vertical arrows indicate simultaneous contraction and extension (large arrow, apical contraction and basal extension coexisted; small arrow, basal contraction and apical extension coexisted). **Bottom:** Changes in the internal diameter at the three parts (symbols are the same as the top figure), changes in the mitral valve ring diameter (MRD: brown dotted line), and changes in displacement of the posterior part of the mitral ring movement (MRM: yellow dotted line). The numbers are the same as those in the top figure. The area filled with the blue color shows the effect of the bellows-like deformation, and that with the orange color, the effect of the pouch-like deformation. PW, posterior wall; IVS, interventricular septum; IS, 1st heart sound; IIs, 2nd heart sound; IC, isovolumetric contraction; Ej, ejection; IR, isovolumetric relaxation; SF, slow filling; AC, atrial contraction; ERF and LRF, early and late rapid filling; pre-ET, pre-ejection transition; post-ET, post-ejection transition; P,Q,R,S,T, ECG symbols.

Table 1
Changes in wall thickness.

PW	A	C	B
Minimum (D) (mm): (Min)	7.5 (St)	6.7	4.8
Maximum (S) (mm): (Max)	12.0	12.0	11.0
Max/Min	1.60	1.79	2.29
(Max/Min) vs A	1.00	1.12	1.43
(Max – Min)/Min	0.60	0.79	1.29
(Max – Min)/Min vs A	1.00	1.32	2.15
(Max – Min)	4.50	5.30	6.20
(Max – Min) vs A	1.00	1.17	1.37
Contracting velocity (mm/s)	17	22	27
(St – Min) (mm)	0.0	–0.8	–2.7
Velocity difference	0	5	10
Contracting velocity vs A	1.00	1.29	1.59

IVS	A	C	B
Minimum (D) (mm): (Min)	7.5	7.3	6.1
Maximum (S) (mm): (Max)	12.0	11.2	9.5
Max/Min	1.60	1.53	1.56
(Max/Min) vs A	1.00	0.96	0.98
(Max – Min)	4.5	3.9	3.4
(Max – Min)/Min	0.60	0.53	0.55
(Max – Min)/Min vs A	1.00	0.88	0.92
Contracting velocity (mm/s)	19	16	12

Wall thickness in the posterior wall (PW) and the interventricular septum (IVS) measured at the three parts [apical(A), central (C) and basal part (B)] in the maximum [systole, Max(S)] and the minimum [diastole, Min(D)] points during one cardiac cycle shown in Fig. 2. Measurement data by the ratio (Max/Min), Max/Min vs A (i.e. Max/Min compared with the same ratio in the Apex), and others are shown. The contraction velocity is referred to estimate the contractility of the local LV wall. St, standard value (7.5 mm: end-diastolic thickness).

LV wall dynamics macroscopically measured

The wall thickness change at the three parts (A, C, B) (Fig. 2 top, Table 1)

The normal myocardial thickness was ca 11–12 mm in the maximum systolic level (Max) in all parts.

Apical part (A) (Fig. 2 top, green line): The PW thickness showed a 60% increase at the maximum from the end-diastolic minimum [i.e. (Max – Min)/Min = (12.0 – 7.5)/7.5 = 0.60] (Table 1, Fig. 2 top, 7.5 = standard thickness; St). The change in the IVS was nearly identical (ca 56%), so that the LV cylindrically shrank, leading to the monotonously concentric wall thickening (see Fig. 3 top left).

Basal part (B) (Fig. 2 top, blue line): The PW thickness change was not simple. It decreased 2.7 mm from 7.5 mm (St) to 4.8 mm during ejection (Ej), although the dimension in this part was enlarged (vide infra). Then it increased 3.5 mm (47% of the St) by the contraction from the isometric relaxation (IR) to the rapid filling (RF) (Fig. 3, bottom B). Thus the basal wall thickness change was not monotonous but biphasic due to the initial thinning followed by the thickening during one cardiac cycle.

Central part (C) (Fig. 2 top, red line): Although the thickness changes were nearly the same as those of the apical part, the maximum contraction to the extending deformation during the RF was ca 3 times faster compared to that in the basal part.

Velocity of muscle contraction in each part (Table 1, contracting velocity):

The increment of the wall thickness was less in the basal part than that in the apical part (47% vs 60%). However, the contracting velocity in the basal part (mm/sec) was greater than that in the apical part (27 mm/s vs 17 mm/s), reflecting the contracting power in the basal part by the contraction added the preload [19,20].

The speed for recovering from 12 mm to the standard thickness in the central part was faster than that in the apical part (67 mm/s

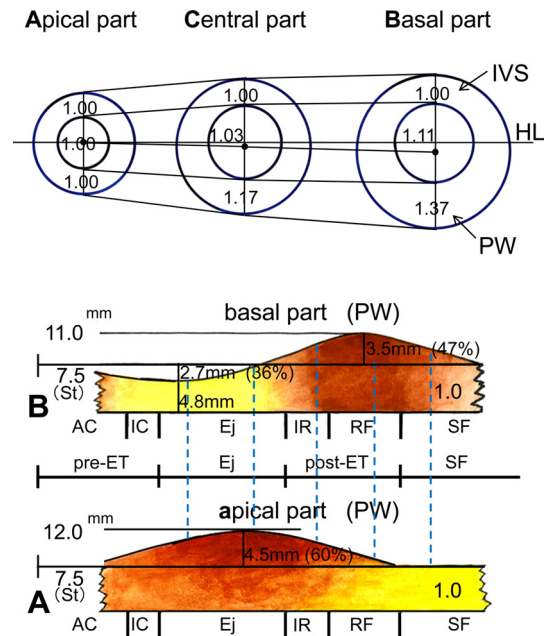


Fig. 3. Schematic representation of the basic deformation. **Top:** Deformation of the LV wall in the short-axis section planes. Schematic figures of Table 1 and Fig. 2, illustrating the changes in the LV wall thickness and internal diameter. Large circles, end-diastole; small circles, end-systole; IVS, interventricular septum; PW, posterior wall; HL, horizontal line. **Bottom:** The time serial thickness change of the posterior wall (PW) at the basal (B) and apical (A) parts. The yellow area shows the extension and the brown, the contraction. AC, atrial contraction; IC, isometric contraction; Ej, ejection; IR, isometric relaxation; RF, rapid filling; SF, slow filling. (St), the standard value (7.5 mm: end-diastolic thickness); pre-ET, pre-ejection transition; post-ET, post-ejection transition.

vs 19 mm/s; Fig. 2, top), indicating the rapid extending deformation in this part during the RF by a part of the bellows movement and the pouch-like deformation with the late systolic basal contraction.

Specificity of the IVS: The IVS thickness increase during contraction in all three parts (A, C, and B) was almost identical. This was evidenced by the ratio of (Max/Min)/Ap (= from 1.00 to 0.96) (Table 1, bottom). Contrary to the PW, there was no biphasic thickness change in the basal part. So, the behavior of the IVS was considerably different from that of the free wall and was intrinsic to the eccentric deformation in the basal part of the LV during Ej.

Time serial changes of the PW thickness (Fig. 2 top, Fig. 3)

The PW increase in thickness (contraction) at the **apical part (A)** started in the early pre-ejection transitional period (pre-ET) coincident with the P wave of the electrocardiogram from the endocardial side of the LV wall and reached the maximum in the middle of Ej (Fig. 3, bottom A). Then it decreased (extension) gradually toward the late rapid filling (RF). Thus, the apical part had its contraction up to the mid Ej followed by the extension. Thereafter, there was no remarkable change (Fig. 3, bottom A: SF period).

On the contrary, the thickness in the **basal part (B)** unexpectedly began to decrease (extension) from the early pre-ET, and reached the minimum in the early Ej period (Fig. 3, bottom B). The thickness increase, which was delayed, began in the late Ej toward the late RF (LRF) and gradually returned to the initial thickness.

Observing the correlation between the time serial changes, the apical contraction (thickness increase) and the basal extension (thickness decrease) of the PW occurred coincidentally during the Ej phase (Fig. 2 top, large vertical red arrow), and further the apical extension occurred simultaneously with the basal contraction

Table 2
Changes in internal diameter.

	A	C	B	(B - A) _{Ej}	(B - A) _{RF}
Maximum (D) (mm): (Max)	39.0	42.5	49.0	10	12
Minimum (S) (mm): (Min)	32.0 (St)	33.0	35.5	3.5	3.5
Max vs A	1.00	1.09	1.26		
Min vs A	1.00	1.03	1.11		
(Max - Min)	7.0	9.5	13.5		
(Max - Min)/Min	0.22	0.29	0.38		
(Max - Min)/Min vs A	1.00	1.32	1.73		
Max/St	1.22	1.33	1.53	2.9	3.4
(Max/St) vs A	1.00	1.09	1.25		
Contracting velocity (mm/s)	52	54	26		

Internal diameter changes of the left ventricle (LV) at the three parts (Table 1) in the maximum [diastole, Max(D)] and the minimum [systole, Min(S)] points during one cardiac cycle in Fig. 2.

A, apical data; St, standard value (32.0 mm: end-systolic diameter); (B - A)_{Ej}, difference between B and A at the IC phase; (B - A)_{RF}, difference between B and A at the end of the RF point.

during the LRF phase (Fig. 2 top, small vertical red arrow). This indicated the non-uniform contraction of the PW.

Discrepant changes in the LV wall thickness and the concept of peristalsis

As shown in Fig. 2 top, and schematically shown in Fig. 3 bottom, the wall contraction started from the apex and was followed by the delayed basal contraction. Namely, the contraction transmitted from the apical part to the basal part. The onset, the maximum, as well as the end of the contraction of the PW and IVS occurred at the apical (A), central (C) and basal (B) parts in this order. This confirmed the presence of the “peristalsis” of the PW and the IVS.

The time discrepancy in the maximum thickening between the apical and the basal part in the PW was about 210 ms (A - C = 120 ms, C - B = 90 ms) and about 180 ms in the IVS (Fig. 2, top).

Changes in the LV internal diameter and the sequel (extruding deformation)

Changes at the three parts of the LV (Fig. 2, bottom, Fig. 3, Table 2)

Another feature of LV deformability was the effects of the changes in the internal diameter. The measured data for each part are shown in Table 2, where the Max(D) is the so-called maximum end-diastolic, and the Min(S), the minimum end-systolic dimensions.

As each diameter changed concomitantly with the wall thickness changes, the shape of the LV and also the mitral valve (vide infra) were obliged to change as schematically shown in Fig. 4.

When compared with the apical part during so-called diastole, the Max(D) in the central and basal parts was bigger by 9% and 26%, respectively; however, the Min(S) during so-called systole was smaller in C and B, i.e. only 3% and 11%, respectively (Fig. 2; shaded blue area). This indicated much more dilatation in the central and basal parts during the apical end-systolic phase, the increase of which was 32% (part C) and 73% (part B). Thus, the contraction of the LV wall was not equal, indicating that the apical contraction promoted the rather “systolic” dilatation, particularly in the basal part.

Moreover, central diameter [Min(S)] (Fig. 2, middle; red line) was transiently less than that of the apical part (green line) during the late systolic phase, indicating the “systolic extruding deformation” toward the LV cavity. Also, it should be mentioned that the central and basal PW were still continuing to thicken

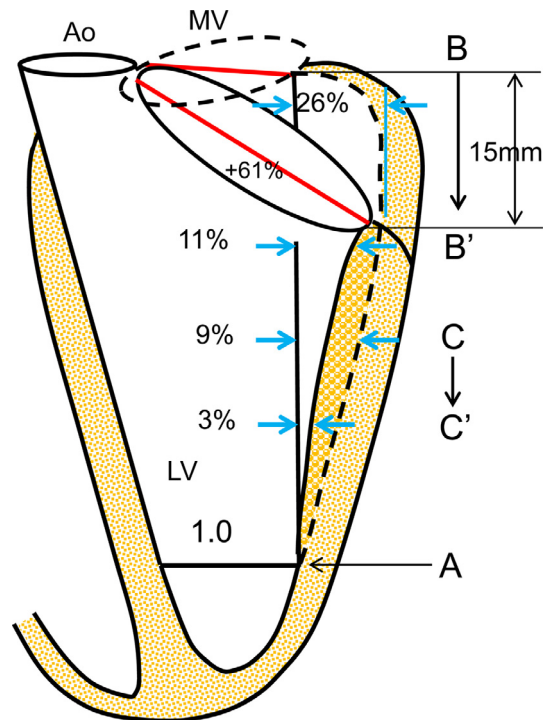


Fig. 4. Schema represents the deformability of the posterior wall and the mitral ring in the long-axis direction. A, B, and C, end-diastolic points at the apical (A), basal (B), and central (C) parts; B', C', end-systolic points (Apical point is fixed); during cardiac cycle, the points B (basal) and C (central) move to the points B' and C'. The change in the internal diameter during systole is depicted by the distance between the paired blue arrows in the Max and Min at points B and C (cf. Table 2). The percentage numbers (%) are the changing ratios to the apical diameter (A). Red line is the mitral ring diameter (long: systole, short: diastole), broken line: period of extension, +61% = increment of the ring diameter during systole compared with that at the endo-diastole. Ao, aorta; MV, mitral valve; LV, left ventricle; orange colored area, LV wall and interventricular septum.

beyond the IR, while the diameters of these parts were increasing at the same time.

Time serial change of the internal diameter in the LV (Fig. 2, bottom)

The difference in the diameter between the apical (green line) and the basal parts (blue line) was about 10 mm in the IC period, but it decreased rapidly to about 3.5 mm in the RF period (blue color area). The nearly parallel movement of these two lines was due to volume change and was regarded as the “bellows-like deformation” during the LV contraction.

Thereafter, this difference rapidly increased toward the SF period due to the LV filling (orange color area) followed by the gentle expansion of all parts.

Among them, it is of note that there was a rather rapid increase in the diameter of part C, which indicated the prompt recovery from the extruding deformation described above, which will be related to the RF described below.

When the thickness in the basal part of the PW was at the maximum during the LRF the apical and central parts were at the minimum (Fig. 2, top), indicating the inevitable expansion of these parts.

Changes in the mitral valve ring diameter (MRD) and the valve ring movement (displacement: MRM)

Changes in the diameter (brown line in Fig. 2, bottom; MRD)

The MRD increased in average from ca 15.4 mm in the IC to ca 25.0 mm in the end of the early RF (ERF) during Ej (ca 61% increase).

Then, it rapidly decreased during the late RF (ca 18 mm; about 40%) followed by the further decrease (about 20%) toward the next IC.

Systolic increment of the MRD resulted in the increase in the surface area of the valve ring and then the volume of the left atrium (LA). The change in the ring configuration from circular to oval and the rapid upward movement of the ring during the RF caused the LV swallowing action to the intra-atrial blood. This is the “**pouch like**” action (Fig. 4).

Displacement of the posterior part of the mitral valve ring (MRM)

The mitral ring moved ca 15 mm downward during the Ej (yellow line in Fig. 2, bottom) and reached the lowest level at the early RF (Fig. 4B–B’, a part of the **bellows action**). At this time, the maximum contraction of the central part in the PW appeared. When the muscle showed the maximal contraction in the basal part, rapid upward movement of the ring accompanied with the rapid expansion of the central part of the LV occurred during the RF (recovering from the extruding deformation of the LV) and reached the upper level at the end of the late RF. Then the maximum displacement (ca 24 mm) was seen at the atrial contraction (AC).

When the maximum PW contraction at the basal part appeared concomitant with the relaxation at the central and apical parts (Fig. 2 top; LRF), the rapid MRD decrement and the rapid increment of the MRM were observed (Fig. 2 bottom; LRF). These results were reflected in the “**sphincter-like** action” surrounding the inflow orifice and the “**pouch-like** deformation” in the basal part together with the **hinge movement** of the mitral valve ring (ca 15 mm) (Fig. 4).

Correlation between the LV deformability and the non-uniformity of the myocardial C/E property

Fig. 5 is a modification of the figure from the previous paper [36]. It was demonstrated that the C/E property estimated by the aSR distribution spatially and time sequentially was unexpectedly very complex. Myocardial contraction and extension were not always cooperative and the synergism of the muscle fibers was not necessarily present in every muscle layer in the same location of the LV wall.

The “toned” distribution (Fig. 5B, iii), where the “regional” myocardium had a different magnitude (intensity) of the aSR, was

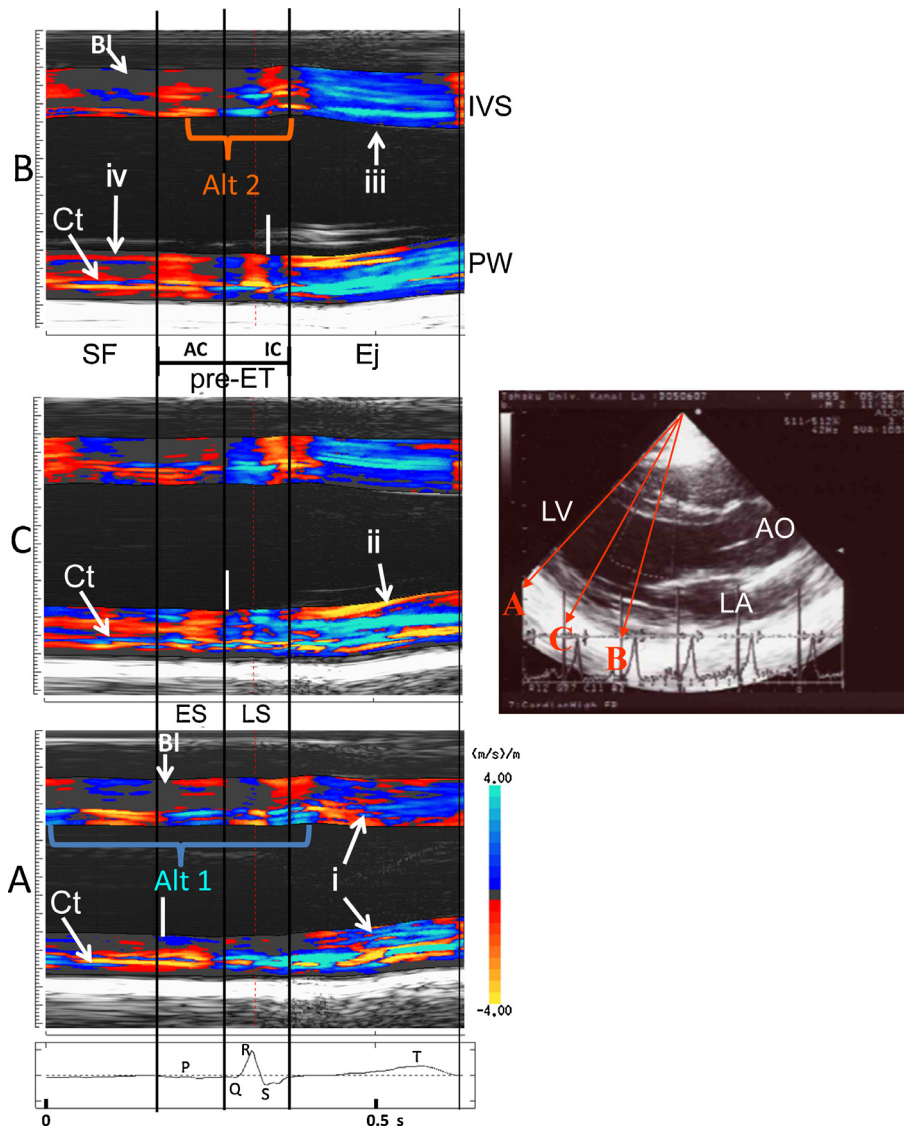


Fig. 5. M-mode aSR distribution images obtained at three points (B: basal, C: central and A: apical) during the slow filling (SF) through the ejection (Ej). The aSR distribution data obtained simultaneously in the three beam directions (red lines on the 2D echocardiogram). i, ii, iii, iv, BI, classification of the spatial aSR distribution pattern; i, spotted; ii, multi-layered; iii, toned; iv, stratified; BI, relaxation; ES, early stage; LS, late stage; Alt 1, Alt 2, alternating 1, alternating 2; Ct, contracting superficial cardiac muscle; AC, atrial contraction; IC, isometric contraction; Ej, ejection; IR, isometric relaxation; RF, rapid filling; SF, slow filling. (St), the standard value (7.5 mm: end-diastolic thickness).

observed in the Ej, resulting in the monotonous deformation of the basal PW and IVS.

The “multi-layered” distribution (Fig. 5C, ii) showed the simultaneously contracting and extending muscles. Namely, the opposite aSR was piled up on the other. This was observed in the apical and central PW during the IC and the Ej.

Of the mixed pattern, the “spotted” distribution (Fig. 5A, i) appeared during the Ej in the apical part, and the “stratified” distribution (Fig. 5B, iv) was seen in the SF.

In between SR(+) and SR(–), there was the widely spread distribution BI (black zone), where neither contraction nor extension was observed. Namely, the muscle fiber was nearly or completely relaxed (real relaxation) during either diastole or even systole. Thus the myocardial muscles essentially had non-uniform activities.

Discussion

Since the era of M-mode echocardiography, we have noticed that the timings of the maximal systolic contraction of either the IVS or the PW are not simultaneous [36] and usually the peak of intrusion of the PW into the LV is slightly delayed. Such a non-uniform change in the length or thickness of the myocardial fiber was verified in the present study. In fact, this induces the distortion of the myocardial tissue [35,36] and so deforms the wall [1,2].

This deformation is three-dimensional, therefore, the numerous short-axis sections perpendicular to the long-axis plane were three dimensionally stocked from the apex to the base and these constituted the fundamental measurement source of the present study. The study of the macroscopic (muscle layer) and the microscopic (muscle fiber) levels afore-mentioned [8,27,30] disclosed three types of deformation named (1) basic, (2) combined, and (3) integrated deformations which constitute the LV wall dynamics.

The significance of the basic deformation (Figs. 3 and 4)

The macroscopic study included the change in the LV wall and the mitral valve deformity. First, the thickness change in the IVS was slight, whereas change in the free wall (represented by the PW) was quite different.

Namely, the wall thickening was concentric and monotonous at the apical part, while it was biphasic in the basal part (Fig. 3, bottom). Furthermore, the behavior of the central part was in between them, i.e. the extruded deformation toward the LV cavity during systole followed by the brisk rebound during diastole.

It is of note that, contrary to expectation, the “systolic thickening” and the “diastolic thinning” of the LV wall do not necessarily indicate the classically defined “systole” and “diastole”, respectively. At the time of the apical thickening, which started prior to the classical systole, the basal part showed thinning even during classical systole. Also, the division of the contraction and the extension differs depending on the part of the LV wall. During classical systole, both contraction and extension in the LV wall coexisted. Also during classical diastole, the same was true, i.e. the LV extension and contraction co-existed. Therefore, the division of the systole and diastole in a sense of classic cardiac physiology is nothing but the clinical use, i.e. electrocardiogram, direct or indirect pressure tracings or heart sounds and phonocardiogram.

The simultaneous LV internal diameter change observed in the long-axis section was also important. Concomitant with the systolic downward displacement of the lateral side of the mitral ring and the enlarged circular deformation, there was the extruded PW deformation of the central part toward the LV cavity (Fig. 4).

This was associated with the greatly enlarged internal diameter of the basal part which helped the bellows action described below. In the late systole, the decreased valve ring diameter and the abrupt upward displacement (sphincter movement) caused the pouch-like deformation.

The basal part played an important role. Combined with the large change in the internal diameter on the one hand and relatively small thickness change on the other hand, this part works just like the controller for blood flow volume and structure with high mechanical efficiency regarding the LV function. This importance, however, has not been discussed yet by anyone.

The apical part played an important role as the generator and controller of the intra-ventricular pressure. This was evidenced by the big thickness change and relatively small diameter change.

The work of the central part (mid-ventricular portion) was just like the hinge of the PW movement. In between the apical and basal parts, the accelerating ejection was enhanced by its “bellows like” effect, and also the suction effect [36] for the mitral inflow was introduced by the extrusion during the RF phase.

The significance of the combined deformation

This is just like an extended spectrum of the basal deformation by adding the microscopic C-R/E properties using the aSR.

Peristaltic deformation

This peristaltic deformation is confirmed by the apical to basal transition of the contraction with the appropriate time lag (210 ms in the normal case) (Fig. 2). This is reasonable to understand the squeezing effect of the LV during the systolic phase [32] and the suction effect in the diastolic phase [36].

Bellows-like deformation

The aSR study disclosed that in the Ej phase, the contraction of the PW progressed from the epicardial side to the endocardial side and that of the IVS, from the right ventricular (RV) side to the LV side. The extrusion of the central PW into the LV cavity and the various mitral ring movements, both assist the eccentric deformation (Fig. 6, Ej), resulting in the bellows-like movement which gives the forceful LV ejection [32] (the area filled with the blue color in Fig. 2).

Pouch-like deformation

In the late Ej and post-ET period (basal contraction and apical extension coexist), the special form of the deformation named “pouched-like” was seen [35,36] (Fig. 6 LS-ERF, LRF). Thereafter, the rapid LV dilatation occurs by the movement of the apical and the central parts (Fig. 6 LRF-SF). Meanwhile, the paravalvular muscle acts as the sphincter to the inflow orifice which occurs with the elliptical deformation of the mitral ring. This rather unique pouch-like deformation is valuable to swallow the mitral inflow by the sucking effect of the LV [37] during the RF (Fig. 6 SF).

The integrated deformation

As previous reports stated [35,37], the cardiac cycle is composed of four phases. The overlap of the contraction and the extension exists, and in total, the length of contraction and extension is equal. The overall deformation is the integrated deformation, as schematically shown in Fig. 6, and which is brought up *en bloc* on the right column.

Fig. 6 shows the sequence of the wall movement due to the deformation. In the right column, blue arrows indicate the

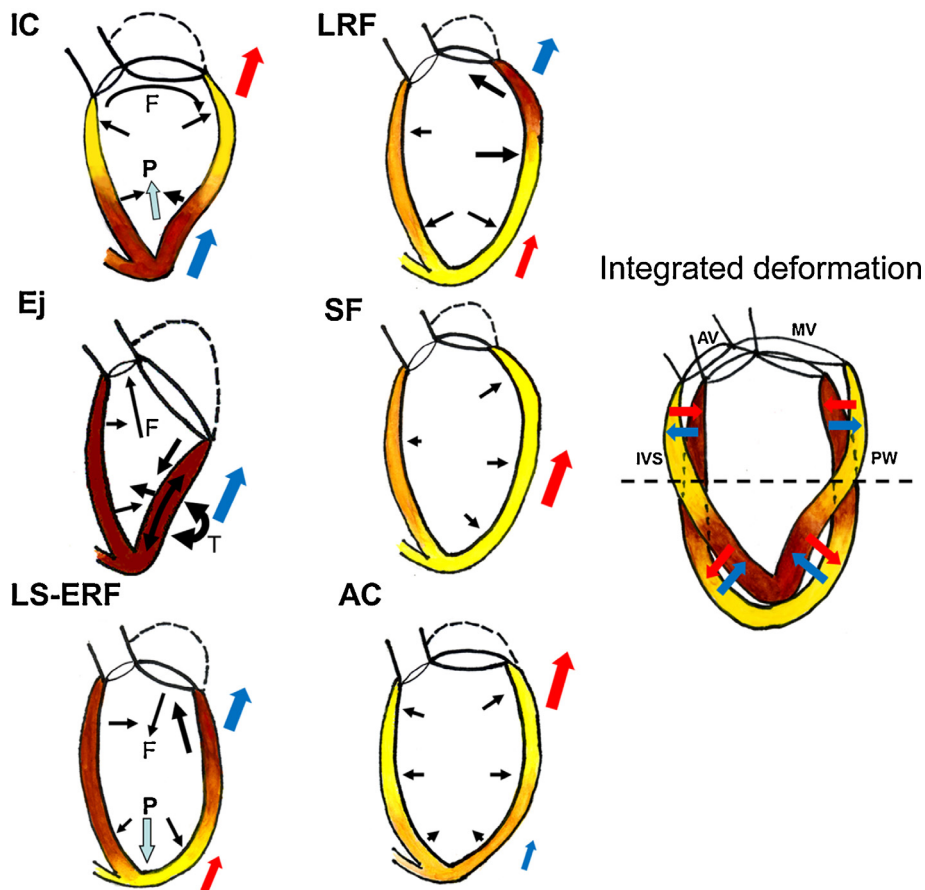


Fig. 6. Schematic representation of the LV deformability in the longitudinal section plane during a cardiac cycle. Left column shows the propagating process of the contraction (blue thick arrows), and middle column, the extension (red thick arrows) propagate from the apical to the basal parts. Yellow area, extending area; brown area, contracting area; orange area, tension area; blue thick arrows, magnitude of contraction; red thick arrows, magnitude of extension; black arrows, direction and magnitude of displacement of the wall; thick black arrow T, circumferential tension; light blue arrow P, local pressure change; black arrow F, flow direction; AC, atrial contraction; IC, isometric contraction; Ej, ejection; SF, slow filling; LS-ERF, late systole–early rapid filling; LRF, late rapid filling. Right column: *En bloc* diagram is the overlapping display of the LV in the early systole and diastole showing the integrated deformation of the LV wall during a cardiac cycle. Periodical and reciprocal deformations between the apical and the basal parts are demonstrated. The horizontal dotted line passing through the center signifies an imaginary boundary line of the reciprocal deformation. Details: see the text. Yellow area; extending area, brown area, contracting area; red arrow, deforming direction and magnitude of the LV wall in diastole; blue arrow, deforming direction and magnitude of the LV wall in systole; LV, left ventricular; PW, posterior wall; IVS, inter-ventricular septum; horizontal dotted line, imaginary boundary line; AV, aortic valve; MV, mitral valve.

simultaneous apical contraction and the basal extension during systole, and red arrows, the simultaneous basal contraction and the apical extension during diastole. In between, the dotted line indicates the imaginary boundary zone crossing the central part.

In total, the concrete results of the present study substantially differ from the ordinary physiological concept of LV wall motion.

The LV pressure (P) develops by contraction when the internal diameter decreases (Fig. 6 IC). Simultaneously, however, the basal part dilates producing a large eddy flow in the basal area [32] (symbol F in Fig. 6 IC). Successively, the contractions of the central and basal parts (extruding of the PW) conduct LV ejection (Fig. 6 Ej), and also result in the apical extension (Fig. 6 LS-ERF). The progressive LV dilatation (pouch-like deformation) (Fig. 6 LRF) is followed by the successive and gentle extension (Fig. 6 SF) and then the atrial contraction (Fig. 6 AC).

Whenever this reciprocal deformation occurs periodically during a cardiac cycle, the profile of the LV dynamics will be just like that of a rotary pump with continuous circular movement without any pause or any overload in any specific part. It might play an important role in preventing sudden changes in LV function in either pressure, volume, or heart rate. A disorder of this deformation may produce various mechanical dysfunctions just like the takotsubo cardiomyopathy, although further studies are necessary to obtain clinical implications.

Study limitations

First, the small number of subjects makes it impossible to generalize our results and precludes strong statistical conclusions, although a self-controlled design in this study may have made the results more reliable. The subjects are presumably healthy adults, but a small effect from age differences may not be excluded. Also, it may be more accurate to present high-resolution movie images to better understand the results.

Second, both of the present technologies of “phase difference tracking method in ultrasound” and “high frame rate 2D echocardiography” have not been widely used because they were developed in our laboratory. Therefore, the present results might not be easy to acknowledge particularly to those who adhere to the traditional physiological concept, although the present study does not necessarily deny the previous noninvasive studies.

Third, we did not refer to or compare with the large amount of literature, and could not refer to a comparative study. We postpone our final conclusions.

Conclusions

By using the high frame rate 2D echocardiography and the aSR distribution developed by us, the deformability of the LV

throughout the cardiac cycle was investigated. We found that the non-uniformity of the myocardial contraction and the axial strain rate (aSR) distribution of the myocardial fibers were the principal determinants of LV deformability. Based on these observations, the following three types of deformations were established, i.e. basic, combined, and integrated deformations. The integrated deformation seemed to have the identical mechanism to a rotary pump and was regarded as the final feature of the smooth, tireless, and quite efficient cardiac beat.

Funding

This research received no grant from any funding agency in the public, commercial, or not-for-profit sectors.

Conflict of interest

The authors declare that there is no conflict of interest.

References

- [1] Brutsaert DL. Nonuniformity: a physiologic modulator of contraction and relaxation of the normal heart. *JACC* 1987;9:341–8.
- [2] Brutsaert DL, Sys SU. Relaxation and diastole of the heart. *Physiol Rev* 1989;69:1228–315.
- [3] Schoepfoerster RT, Silva CL, Ray G. Evaluation of left ventricular function based on simulated systolic flow dynamics computed from regional wall motion. *J Biomech* 1994;27:125–36.
- [4] Bogaert J, Rademakers FE. Regional nonuniformity of normal adult human left ventricle. *Am J Physiol Heart Circ Physiol* 2001;280:610–20.
- [5] Shapiro E, Marier DL, St John Sutton MG, Gibson DG. Regional non-uniformity of wall dynamics in normal left ventricle. *Br Heart J* 1981;45:264–70.
- [6] Miyatake K, Yamagishi M, Tanaka N, Uematsu M, Yamazaki N, Mine Y, Sano A, Hiram M. New method for evaluation of left ventricular wall motion by color-coded tissue Doppler imaging: in vitro and in vivo study. *JACC* 1995;25:717–24.
- [7] Tanaka M. Usefulness of ultrasonic imaging in medical field. In: Shimizu H, Chubachi N, Kushibiki J, editors. *Acoustical imaging*, vol. 17. New York: Plenum Press; 1989. p. 453–66.
- [8] Tanaka M. Historical perspective of the development of echocardiography and medical ultrasound. In: Schneider SC, Levy M, McAvoy BR, editors. *Proceedings of the IEEE Ultrasonics Symp.*, 2002 IEEE, vol. 2. New York: IEEE Inc.; 1998. p. 1517–24. Available: <http://www.ieee-uffc.org/ultrasonics/teaching/us0000.pdf>.
- [9] Sato Y, Maruyama A, Ichihashi K. Myocardial strain of the left ventricle in normal children. *J Cardiol* 2012;60:145–9.
- [10] Nishimura K, Okayama H, Inoue K, Saito M, Yoshii T, Hiasa G, Sumimoto T, Inaba S, Ogimoto A, Funada J, Higaki J. Direct measurement of the radial strain in the inner-half layer of the left ventricular wall in hypertensive patients. *J Cardiol* 2012;59:64–71.
- [11] Suzuki K, Akashi Y, Mizukoshi K, Kou S, Takai M, Izumo M, Hayashi A, Ohtaki E, Nobuoka S, Miyake F. Relationship between left ventricular ejection fraction and mitral annular displacement derived by speckle tracking echocardiography in patients with different heart diseases. *J Cardiol* 2012;60:55–60.
- [12] Arts T, Veenstra PC, Reneman RS. Epicardial deformation and left ventricular wall mechanics during ejection in the dog. *Am J Physiol* 1982;243:H379–90.
- [13] Myers JH, Stirling MC, Choy M, Buda AJ, Gallager KP. Direct measurement of inner and outer wall thickening dynamics with epicardial echocardiography. *Circulation* 1986;74:164–72.
- [14] Sabbah HN, Marzilli M, Stain PD. The relative role of subendocardium and subepicardium in left ventricular mechanics. *Am J Physiol Heart Circ Physiol* 1981;240:920–7.
- [15] Gallagher KP, Osakada G, Matuzaki M, Miller M, Kemper WS, Ross Jr J. Non-uniformity of inner and outer systolic wall thickening in conscious dogs. *Am J Physiol Heart Circ Physiol* 1985;249:241–8.
- [16] Derumeaux G, Ovize M, Loufoua J, Pontier G, Andre-Fouet X, Gribier A. Assessment of nonuniformity of transmural myocardial velocity by color-coded tissue Doppler imaging: characterization of normal, ischemic, and stunned myocardium. *Circulation* 2000;101:1390–5.
- [17] Kilner PJ. Our tortuous heart in dynamic mode – an echocardiographic study of mitral flow and movement in exercising subjects. *Heart Vessels* 1997;12:103–10.
- [18] Watanabe H, Hisada T, Sugiura S, Okada J, Fukunari H. Computer simulation of blood flow, left ventricular motion and their interrelationship by fluid-structure interaction finite element method. *JSMEJC* 2002;45:1003–12.
- [19] Ishida N, Takishima T. Dynamics of the myocardium. In: Ishida N, Takishima T, editors. *Cardiodynamics and its clinical application*. 2nd ed., Tokyo: Bunkodo; 1992. p. 1–63.
- [20] Braunwald E, Sonnenblick EH, Ross Jr J. Contraction of the normal heart. In: Braunwald E, editor. *Heart disease*. 2nd ed., Philadelphia: WB Saunders; 1984. p. 409–46.
- [21] Matsumoto T, Komori R, Mashima H. The functional morphology of the heart & mechanical performance of the myocardium. In: Matsuda K, editor. *Physiology of circulation: Japanese handbook of physiology*, vol. III. Tokyo: Igakushoin Ltd.; 1969. p. 70–147.
- [22] Barnett VA. Cardiac myocytes. In: Iaizzo PA, editor. *Physiology and devices: handbook of cardiac anatomy*. Part III. New Jersey: Humana Press; 2005. p. 113–21.
- [23] Sonnenblick EH, Ross Jr J, Covell JW, Spotnitz HM, Spiro D. The ultrastructure of the heart in systole and diastole: changes in sarcomere length. *Circ Res* 1967;21:423–31.
- [24] Rushmer RF. Functional anatomy and control of the heart. In: Rushmer RF, editor. *Cardiovascular dynamics*. 4th ed., Philadelphia: WB Saunders; 1970. p. 76–131.
- [25] Tanaka M, Kanai H, Sato M, Chubachi N. Measurement of the moving speed of local myocardial tissue by using the phase difference tracking method and its clinical significance. *J Cardiol* 1996;28(Suppl.):163.
- [26] Kanai H, Hasegawa H, Chubachi N, Koiwa Y, Tanaka M. Non-invasive evaluation of spatial distribution of local instantaneous strain energy in heart wall. In: Lees S, Ferrari LA, editors. *Acoustic imaging*, vol. 23. New York: Plenum Press; 1997. p. 187–92.
- [27] Kanai H, Hasegawa H, Chubachi N, Koiwa Y, Tanaka M. Noninvasive evaluation of local myocardial thickening and its color-coded imaging. *IEEE Trans Ultrason Ferroelectr Freq Control* 1997;44:752–68.
- [28] Kanai H, Tanaka M. Minute mechanical-excitation wave-front propagation in human myocardial tissue. *J Appl Phys* 2011;50. 07HA01-7.
- [29] Yoshiara H, Hasegawa H, Kanai H, Tanaka M. Ultrasonic imaging of propagation of contraction and relaxation in heart walls at high temporal resolution. *J Appl Phys* 2007;46:4889–96.
- [30] Ohtsuki S, Tanaka M. The flow velocity distribution from the Doppler information on a plane in three-dimensional flow. *J Vis* 2006;9:69–82.
- [31] Ohtsuki S, Tanaka M. Doppler pressure field deduced from the Doppler velocity field in an observation plane in a fluid. *Ultrasound Med Biol* 2003;29:1431–8.
- [32] Tanaka M, Sakamoto T, Sugawara S, Nakajima H, Katahira Y, Ohtsuki S, Kanai H. Blood flow structure and dynamics, and ejection mechanism in the left ventricle: analysis using echo-dynamography. *J Cardiol* 2008;52:86–101.
- [33] Tanaka M. In: Tanaka M, editor. *Ultrasonic diagnosis of the heart*. 1st ed., Tokyo: Medic ElectroTimes; 1978.
- [34] Tanaka M, Dunn F. Acoustic properties of the fibrous tissue in myocardium and detectability of the fibrous tissue by echo method. In: Dunn F, Tanaka M, Ohtsuki S, Saijo Y, editors. *Ultrasonic tissue characterization*. Tokyo: Springer-Verlag; 1996. p. 231–43.
- [35] Tanaka M, Sakamoto T, Sugawara S, Katahira Y, Tabuchi H, Nakajima H, Kurokawa T, Kanai H, Hasagawa H, Ohtsuki S. A new concept of the contraction-extension property of the left ventricular myocardium. *J Cardiol* 2014;63:313–9.
- [36] Tanaka M, Sakamoto T, Katahira Y, Tabuchi H, Nakajima H, Kurokawa T, Kanai H, Hasegawa H, Ohtsuki S. Non-uniform distribution of the contraction/extension (C-E) in the ventricular myocardium related to the myocardial function. *J Cardiol* 2014;64:401–8.
- [37] Tanaka M, Sakamoto T, Sugawara S, Nakajima H, Kameyama T, Tabuchi H, Katahira Y, Ohtsuki S, Kanai H. Physiological basis and clinical significance of left ventricular suction studied using echo-dynamography. *J Cardiol* 2011;58:232–44.